

FACTORS AFFECTING FLUORESCENT INTENSITY OF Fe₃O₄-CYANINE 5.5 NANOPARTICLES

Le Thi Thu Huong^{1,2}, Phan Ke Son¹, Ung Thi Dieu Thuy¹, Tran Thi Lan Anh¹,
Dong Thi Nham¹, Ha Phuong Thu^{1,*}

¹*Institute of Materials Science, Vietnam Academy of Science and Technology,
18 Hoang Quoc Viet, Cau Giay, Ha Noi, Viet Nam*

²*Vietnam National University of Agriculture, Trau Quy, Gia Lam, Ha No, Viet Nam*

*Emails: thuhp@ims.vast.ac.vn

Received: 29 March 2021; Accepted for publication: 26 November 2021

Abstract. In the diagnosis and treatment of cancer, the nano drug delivery systems have been intensively researched for many years because they are capable of concentrating drugs at the target for a longer time, while protecting other tissues in the body. Recently, fluorescent-magnetic nanomaterials have attracted much attention from researchers in biomedicine due to these multifunctional nanomaterials have great prospects for application in multimodal biomedical imaging in combination with chemotherapy and hyperthermia. However, the factors affecting fluorescent intensity of fluorescent magnetic nanomaterials have not been investigated. In this study, we examined the dependence of fluorescent intensity on different factors in the synthesis process of Fe₃O₄-cyanine 5.5 nanoparticles. The results showed that Fe₃O₄ nanoparticles needed to be covered with a layer of NH₂ group before reacting with cyanine 5.5-NHS ester. The best cyanine 5.5 NHS ester : Fe₃O₄ and cyanine 5.5 NHS ester : APTES ratios were 1 : 20 and 1 : 3, respectively. The drug delivery did not affect much the fluorescent property while increasing the excitation wavelength could lead to an increase in the fluorescent intensity of the system. These results are the basis to continue to evaluate the potential of Fe₃O₄-cyanine 5.5 nanoparticles in further *in vitro* and *in vivo* biological tests.

Keywords: fluorescent intensity, Fe₃O₄ nanoparticles, cyanine 5.5.

Classification numbers: 2.1.1, 2.2.1, 2.4.3.

1. INTRODUCTION

Optical imaging has been a major cornerstone of histology, biological assays and microscopes for decades because of the high spatial resolution and exceptional detection sensitivity of this method. In particular, multi-channel images distinguish optical images from other imaging methods. Due to the large optical image window, typically between 400 and 1200 nm, it is possible to use multiple fluorescence probes in a single experiment without significant inconsistencies between image channels. Hence, fluorescence imaging has great potential to facilitate the observation of multiple molecular targets in cells and tissues [1].

Fluorescence imaging, as opposed to white light imaging, can be used to visualize the surface tissue and a high signal/background ratio can be achieved in marked tissue. To observe the penetration of drugs inside the cell, fluorescent molecules have also been attached to the drug delivery system. Binding fluorescent molecules (fluorophore) such as fluorescein (emitting green) or rhodamine (emitting red) to materials to locate and observe their distribution in biological experiments has been implemented for many years. However, these fluorescent molecules had weak luminescent intensity and were blurred after a few minutes of operation [2]. Another challenge with fluorescence imaging is the spontaneous fluorescence of body tissues within the visible region of the electromagnetic spectrum. Therefore, a new class of fluorescent molecules that emit in the near-infrared (NIR) region (650-1000 nm) has attracted much attention from scientists, as they give low background signals and relatively deep penetration into the biological matrix [3, 4].

Recently, fluorescent-magnetic nanoparticles have been well investigated for multimodal imaging applications [5, 6]. In the studies, the near-infrared fluorescent fluorophore, cyanine 5.5 (Cy5.5), was used for labeling the presence of nanoparticles in cells.

Many studies have shown that nanosystems containing magnetic particles often have reduced fluorescent intensity (quenching effect) due to the presence of Fe_3O_4 [2]. A study has developed a highly sensitive detection of nucleolin based on the magnetic separation-assistant fluorescence resonance energy transfer inhibition strategy by using Cy5.5-AS1411 as the donor and Fe_3O_4 -polypyrrole core-shell nanoparticles as the NIR quenching acceptor [7].

In some previous studies, we have reported the synthesis and biomedical application of some magneto-fluorescent nanosystems [8 - 10], however, their fluorescent intensity was not much focused.

In a study on the decay fluorescent intensity of orange acridine, a typical fluorescent dye, in the presence of magnetic Fe_3O_4 nanoparticles at different concentrations from 0 to 6250 ng/mL, it was found that at concentrations of Fe_3O_4 nanoparticles lower than 0.0625 ng/mL, the fluorescent intensity decreased sharply as the concentration of Fe_3O_4 nanoparticles increased. In the range of Fe_3O_4 nanoparticle concentrations from 0.0625 to 1.25 ng/mL, the fluorescent intensity of orange acridine decreased linearly as the nanoparticle concentration increased; and when the concentration of Fe_3O_4 nanoparticles exceeded 1.25 ng/mL, fluorescence was essentially undetectable. These findings suggested that magnetic fluorescent composites with optimized fluorescence properties could be obtained by carefully controlling the Fe_3O_4 nanoparticle composition, which provided a better understanding of the interaction between magnetic nanoparticles and luminescence of fluorescent molecules [11].

Although the effect of Fe_3O_4 concentration on fluorescent intensity have already investigated, other factors like polymer coating method, nanoparticle composition, excited wavelength, etc. have not been studied. In this study, we synthesized different Fe_3O_4 -Cyanine 5.5 nanosystems in order to determine how the synthesis parameters affected the fluorescent intensity of the nanosystems.

2. MATERIALS AND METHODS

2.1. Materials

Iron (III) chloride hexahydrate ($\text{FeCl}_3 \cdot 6\text{H}_2\text{O}$), iron (II) chloride tetrahydrate ($\text{FeCl}_2 \cdot 4\text{H}_2\text{O}$), ammonia (NH_3), hydrochloric acid (HCl), Doxorubicin HCl, 1-ethyl-3-(3-

dimethylaminopropyl) carbodiimite (EDC), and N-hydroxysuccinimide (NHS) were purchased from Aldrich. Alginate (Alg) with a molecular weight of 10000 was obtained from Sigma-Aldrich. Chitosan, poly (lactide) - tocopheryl polyethylene glycol succinate (PLA-TPGS), (3-Aminopropyl) triethoxysilane (APTES), and phosphate buffered solution (PBS, pH 7.4) were purchased from Merck. Cyanine 5.5-NHS ester was provided by Lumiprobe. The other chemicals were of analytical grade. All chemicals were used without further purification.

2.2. Methods

2.2.1. Synthesis of Fe₃O₄ nanoparticles

Fe₃O₄ nanoparticles were synthesized by the co-precipitation method of Fe²⁺ and Fe³⁺ salts by NH₄OH, according to the reaction equation:



Specifically, Fe²⁺ and Fe³⁺ salts were accurately weighed in a molar ratio of 1 : 2 and dissolved in 35 mL of 2 M hydrochloric acid to limit the hydrolysis of the iron salts. The mixture was put into a 3-neck flask. Before the reaction, N₂ was pumped into the flask for 20 min to remove all the air. 2 M NH₃ solution was slowly added to the flask (2 drops/s) until the pH of the solution reached around 10 under magnetic stirring condition at 80 °C for 30 min in N₂ atmosphere. The mixture changed in color from the brown to black precipitate. The precipitate was separated by magnet and washed with distilled water to neutral. The precipitate of Fe₃O₄ nanoparticles was then redispersed in distilled water by ultrasonic vibration for 30 min to obtain a 4 mg/mL Fe₃O₄ solution.

2.2.2. Binding Cyanine 5.5

Table 1. Sample compositions (mg/mL).

Sample	Fe ₃ O ₄	APTES	Alginate	Chitosan	PLA-TPGS	Cyanine 5.5-NHS ester
N1	2		1			0.1
N2	2				1	0.1
N3	2			1		0.1
N41	2	0.3			1	0.2
N42	2	0.3			1	0.1
N43	2	0.6			1	0.1
N51	2	0.3	1			0.2
N52	2	0.3	1			0.1
N53	2	0.6	1			0.1
N52D	2	0.3	1			0.1

Fe₃O₄ nanoparticles were bound with cyanine 5.5 according to the following general procedure, with detailed composition shown in Table 1.

10 mg of Cyanine 5.5-NHS ester was dissolved in 5 mL of Dimethylformamide (DMF) to obtain a solution of cyanine 5.5-NHS ester at a concentration of 2 mg/mL. PLA-TPGS was dissolved in tetrahydro furan (THF) solvent to a concentration of 2 mg/mL. Alginate was dissolved in water to a concentration of 5 mg/mL. Chitosan was dissolved in 1 % acetic acid solution to a concentration of 2 mg/mL.

For N1-N3 samples, a polymer solution (Alginate, chitosan or PLA-TPGS) was added to the 4 mg/mL Fe_3O_4 solution according to the determined ratio (Table 1) to obtain the Fe_3O_4 /polymer solution. The mixture was ultrasonically vibrated for 30 min and magnetically stirred for 2 h. The pH of the solution was then adjusted to 8.5 using PBS buffer. Cyanine 5.5-NHS ester solution was added to the mixture and kept stirring for 12 h.

For other samples, APTES was added to the 4 mg/mL Fe_3O_4 solution and allowed to react for 2 h. The pH of the solution was then adjusted to 8.5 using PBS buffer. A solution of cyanine 5.5-NHS ester was added to the mixture and kept stirring for 12 h. Finally, a polymer solution (Alginate, chitosan or PLA-TPGS) was added and kept stirring for another 12 h. Sample N52D was obtained by reacting 0.5 mg/mL Doxorubicin dissolved in activated 2 mg/mL alginate solution with sample N52.

To remove unreacted substances or non-aqueous solvents, the samples were magnetically separated, washed with water and re-dispersed in double distilled water by ultrasonic vibration. Powder samples were obtained by drying the samples after magnetic separation at 60 °C.

2.2.3. The methods of material characterizations

The optical properties of the nanoparticles were determined by fluorescence spectroscopy. An iHR550 spectrophotometer (Horiba) was equipped with a Si-CCD camera cooled by electric heat (Synapse) and the excitation source used was a diode laser with a suitable excitation wavelength, namely 355, 610 or 630 nm. TEM transmission electron microscopy (JEM 1010) and FeSEM field emission scanning electron microscope (Hitachi S-4800) were used to investigate the size and surface morphology of materials. The size distribution and Zeta potential of the FAQ and FAQD were measured in a dynamic light scattering system (DLS) (Nano Zetasizer, Malvern, UK).

3. RESULTS AND DISCUSSION

3.1. Effect of polymer coating on fluorescent intensity

First of all, the samples were investigated using different polymers (alginate, chitosan and PLA-TPGS). These polymers have different characteristic functional groups. Alginate and chitosan are hydrophilic polymers, in which alginate contains OH and COOH functional groups, chitosan contains OH and NH_2 groups, while PLA-TPGS is hydrophobic polymer.

Fluorescence spectra of samples N1, N2, N3 (Figure 1) using 3 respective polymers showed that the fluorescence intensities of these samples were all low, the maximum fluorescence emission wavelength was 690 nm, almost unchanged compared with the original cyanine 5.5-NHS ester. This result showed that if only polymers were used as coatings for Fe_3O_4 nanoparticles, cyanine 5.5 binding was just physical adsorption, fluorescent intensity did not reach the desired value. As for chitosan, although the NH_2 functional group was capable of reacting with cyanine 5.5-NHS ester, chitosan was only soluble in acid medium ($\text{pH} \leq 5$), in which the NH_2 groups were protonated to become NH_3^+ groups that were no longer able to react.

Therefore, in the next experiments, to ensure more efficient binding of cyanine 5.5 to magnetic nanoparticles, APTES was used to attach NH₂ functional groups to the Fe₃O₄ particle surface before being stabilized with the above polymers.

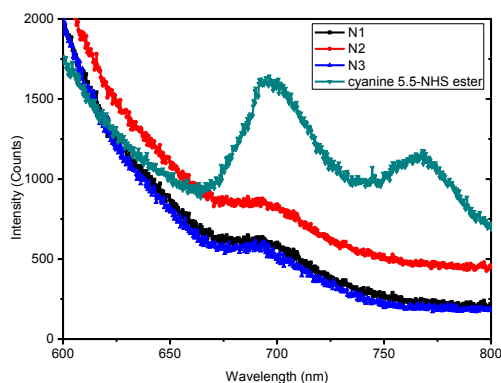


Figure 1. Fluorescent spectra of N1, N2, N3 in comparison with that of cyanine 5.5-NHS ester.

3.2. Effects of APTES and cyanine 5.5-NHS ester concentration

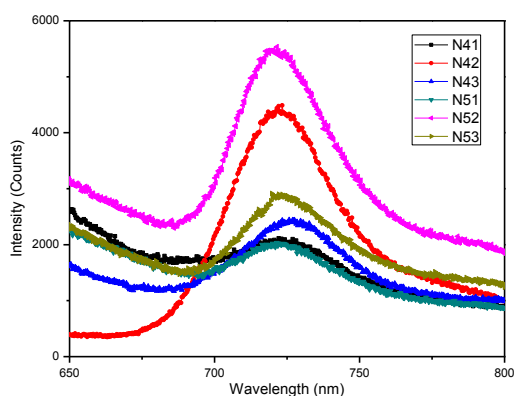


Figure 2. Dependences of fluorescent spectra on APTES and cyanine 5.5-NHS ester.

Fluorescence spectra of samples N41, N42, N43, N51, N52, N53 (Figure 2) showed that the fluorescent intensity directly depends on cyanine 5.5-NHS ester concentration. However, the results showed that the ratio of cyanine 5.5-NHS : Fe₃O₄ = 1 : 10 gave fluorescent intensity much lower than the ratio of 1 : 20 in both N41-N42 and N51-N52 sample series. This result was different from other findings on the relationship between Fe₃O₄ concentration and fluorescent intensity [11, 12]. The results also showed that the concentration of cyanine 5.5-NHS ester involved in the reaction was not a determinant of the fluorescent intensity. This may be related to the number of cyanine 5.5-NHS ester molecules that actually react with the NH₂ groups on the surface of Fe₃O₄ to convert from the NHS ester form to the free cyanine 5.5 with a fluorescence peak at 710 nm. The amount of NH₂ on the surface of Fe₃O₄ particles depends on the concentration of APTES added to the reaction. Therefore, two samples N43 and N53 were continued to fabricate, maintaining the ratio of cyanine 5.5-NHS ester : Fe₃O₄ of 1:20 while increasing the content of APTES to 0.6 mg/mL. However, the fluorescent intensity of these two samples was not higher than that of samples N42 and N52. Thus, the ratio of APTES : cyanine

5.5-NHS ester suitable to achieve the maximum fluorescent intensity was 3 : 1. The fluorescent intensity reached a higher value for the polymer alginate than for PLA-TPGS.

3.3. Dependence of fluorescent spectra on drug delivery process

Sample N52D was resulted from sample N52 by adding Doxorubicin at a concentration of 0.5 mg/mL. Although Doxorubicin is a natural luminescent, it has a weak luminescence intensity in the 450 nm region. It can be seen from Figure 3 that adding Doxorubicin did not affect the fluorescent intensity of the sample at near infrared region. This result proved that this nanosystem could perform many functions such as magnetism, optics and drug carriers simultaneously.

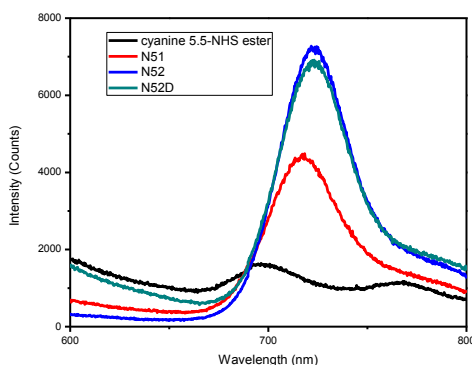


Figure 3. Dependences of fluorescent spectra on drug delivery process.

3.4. Dependence of fluorescent spectra on excitation wavelength

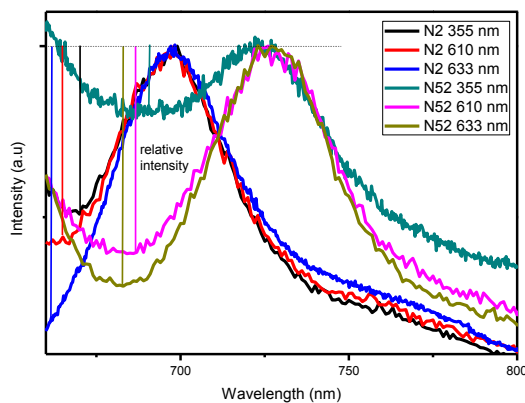


Figure 4. Dependences of fluorescent spectra on excitation wavelength.

Fluorescence spectra of two samples N2 and N52 were recorded at different excitation wavelengths on two devices. In order to compare the spectra recorded on two different devices, they need to be normalized (maximum emitted intensity in units) (Figure 4). Based on the spectral position, it can be seen that the fluorescent intensity depends on the excitation wavelength, the larger the excitation wavelength, the greater the fluorescent intensity. This is completely consistent with the fluorescence theory concerning excitation energy and fluorescence emission [13].

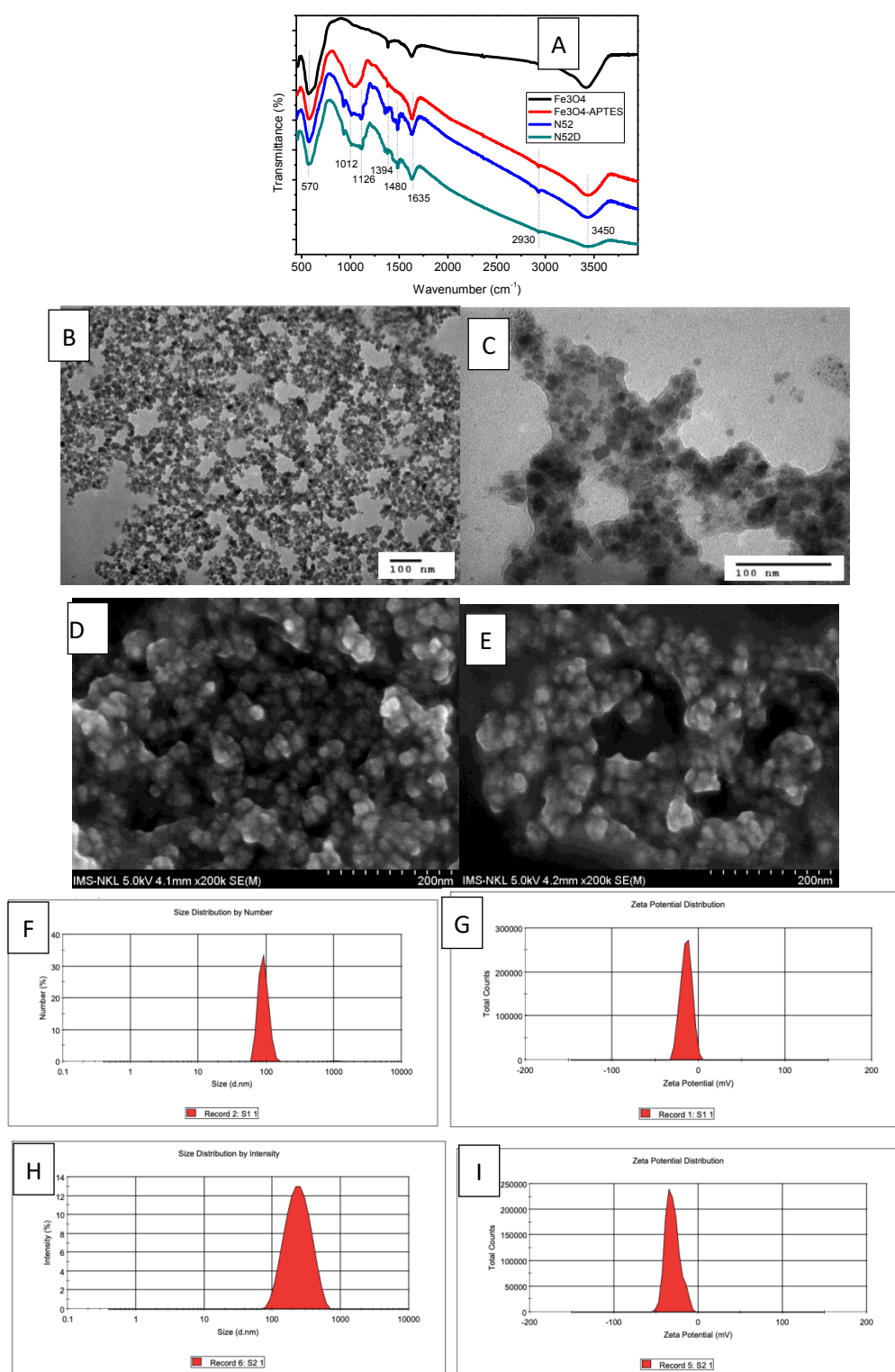


Figure 5. FTIR spectra (A), TEM, FESEM images, size distribution and Zeta potential of N52 (B, D, F, G) and N52D (C, E, H, I).

Thus, in the case of fixed experimental parameters, to enhance fluorescent intensity, the excitation wavelength can be adjusted in the measurements.

Nanosystems with high fluorescent intensity (N52, N52D) were measured for other material properties such as FTIR spectrum, TEM image, FESEM image, particle size distribution and Zeta potential. In Figure 5A, it can be seen that typical peaks appear in the FTIR spectra of the samples. The broad band at 3450 cm^{-1} can be assigned to N-H stretching vibration. The peak at 2930 cm^{-1} is due to the CH_2 groups of APTES and cyanine 5.5. The band at 1012 cm^{-1} is assigned to the Si-O stretching vibration of APTES in the surface of the particles. The peak at 1635 cm^{-1} is assigned to the asymmetric $-\text{COO}$ stretching vibration and the $-\text{NH}_2$ bending vibration. Fe-O bond is observed at about 570 cm^{-1} . The presence of alginate and doxorubicin in samples N52 and N52D was observed by the fine peaks between 1000 and 1600 cm^{-1} . Similar results were recorded in other studies [6, 14]

TEM and FESEM images (Figure 5 B-E) showed that the nanoparticles had a uniform size of about 20 nm. N52D nanoparticles with Doxorubicin appeared on the images with a surrounding polymer layer. This was due to the increased polymer content in this sample when loading Doxorubicin. Figure 5 F-I showed hydrodynamic particle size distribution and Zeta potential of samples N52 and N52D. In aqueous medium, the coating layer of alginate expands so that the size of the particles measured by DLS method is higher than that measured by TEM or SEM. The Zeta potential result also showed that N52 was highly stable with hydrodynamic size below 100 nm. When loading doxorubicin, the hydrodynamic size of N52D significantly increased. This result was consistent with the sample synthesis procedure and the results of TEM and FESEM imagings where a polymeric matrix could be observed. It's also interesting that although N52D had a thicker polymer coating layer, its fluorescent intensity did not change significantly compared to N52. Because nanoparticles at the size range from 30 to 200 nm have been considered as optimal size particles in biomedicine [15], the results also confirmed that these samples were suitable for biomedical applications.

4. CONCLUSIONS

In conclusions, we have successfully fabricated Fe_3O_4 -cyanine 5.5 magnetic-fluorescent nanosystems and determined the most suitable experimental conditions to create the system with the highest fluorescent intensity. It was found that there were 4 factors affecting fluorescent intensity of the nanosystems. First, it is necessary to cover the surface of Fe_3O_4 nanoparticles with NH_2 groups by reaction with APTES. Second, the optimized ratios of components were cyanine 5.5-NHS ester : $\text{Fe}_3\text{O}_4 = 1 : 20$ and cyanine 5.5-NHS ester : APTES = 1 : 3. Third, the process of drug delivery had little effect on the fluorescent intensity of the system. Fourth, the larger the excitation wavelength, the greater the fluorescent intensity. The morphology, size and water dispersion characteristics of the samples with high fluorescent intensity have also been determined. The samples containing Fe_3O_4 nanoparticles with a size of about 20 nm were well dispersed in water, and potential to apply in biomedicine.

Acknowledgements. This work was financially supported by the National Foundation for Science and Technology Development of Vietnam - NAFOSTED under Grant No. 108.05-2019.304 (HPT) and the Vietnam Academy of Science and Technology under Grant No. QTFR01.01/19-20 (HPT).

CRedit authorship contribution statement. Le Thi Thu Huong: Investigation, Data analysis, Writing manuscript. Phan Ke Son: Investigation. Ung Thi Dieu Thuy: Fluorescent measurement and discussion.

Tran Thi Lan Anh: Investigation. Dong Thi Nham: Investigation. Ha Phuong Thu: Methodology: Funding acquisition, Supervision, Manuscript editing.

Declaration of competing interest. The authors declare that they have no known competing financial interests or personal relationships that could have appeared to influence the work reported in this paper.

REFERENCES

1. Pylayeva-Gupta Y. - Near-infrared Molecular Probes for In Vivo Imaging, *Curr. Protoc. Cytom.* **23** (2012) 1-7. <https://doi.org/10.1038/jid.2014.371>.
2. Wang G. P., Song E. Q., Xie H. Y., Zhang Z. L., Tian Z. Q., Zuo C., Pang D. W., Wu D. C., and Shi, Y. B. - Biofunctionalization of fluorescent-magnetic-bifunctional nanospheres and their applications, *Chem. Commun.* (2005) 4276-4278. <https://doi.org/10.1039/b508075d>.
3. Corem-Salkmon E., Perlstein B., and Margel S. - Design of near-infrared fluorescent bioactive conjugated functional iron oxide nanoparticles for optical detection of colon cancer, *Int. J. Nanomedicine* **7** (2012) 5517-5527. <https://doi.org/10.2147/IJN.S33710>.
4. Lian X., Wei M. Y., and Ma Q. - Nanomedicines for Near-Infrared Fluorescent Lifetime-Based Bioimaging, *Front. Bioeng. Biotechnol* **7** (2019) 1-16. <https://doi.org/10.3389/fbioe.2019.00386>.
5. Perillo E., Hervé-Aubert K., Allard-Vannier E., Falanga A., Galdiero S., and Chourpa I. - Synthesis and in vitro evaluation of fluorescent and magnetic nanoparticles functionalized with a cell penetrating peptide for cancer theranosis, *J. Colloid Interface Sci.* **499** (2017) 209-217. <https://doi.org/10.1016/j.jcis.2017.03.106>.
6. Yoo D., Lee C., Seo B., and Piao Y. - One pot synthesis of amine-functionalized and angular-shaped superparamagnetic iron oxide nanoparticles for MR/fluorescence bimodal imaging application, *RSC Adv.* **7** (2017) 12876-12885. <https://doi.org/10.1039/c6ra28495g>.
7. Li Y. R., Liu Q., Hong Z., and Wang H. F. - Magnetic Separation-Assistant Fluorescence Resonance Energy Transfer Inhibition for Highly Sensitive Probing of Nucleolin, *Anal. Chem.* **87** (2015) 12183-12189. <https://doi.org/10.1021/acs.analchem.5b03064>.
8. Thu H. P., Huong L. T. T., Nhung H. T. M., Tham N. T., Tu N. D., Thi H. T. M., Hanh P. T. B., Nguyet T. T. M., Quy N. T., Nam P. H., Lam T. D., Phuc N. X., and Quang D. T. - Fe₃O₄/o-Carboxymethyl Chitosan/Curcumin-based Nanodrug System for Chemotherapy and Fluorescence Imaging in HT29 Cencer Cell Line, *Chem. Lett.* **11** (2011) 1-4.
9. Le T. T. H., Bui T. Q., Ha T. M. T., Le M. H., Pham H. N., Ha P. T. - Optimizing the alginate coating layer of doxorubicin-loaded iron oxide nanoparticles for cancer hyperthermia and chemotherapy, *J. Mater. Sci.* **53** (2018) 13826-13842.
10. Ha P. T., Le T. T. H., Ung T. D. T., Do H. D., Doan B. T., Mai T. T. T., Pham H. N., Hoang T. M. N., Phan K. S., Bui T. Q. - Properties and bioeffects of magneto–near infrared fluorescent nanoparticles on cancer diagnosis and treatment, *New J. Chem.* **44** (2020) 17277-17288. <https://doi.org/10.1039/D0NJ02848G>.
11. Zhang Q., Su R., Wang J. P., and Zhang, Q. - Influence of magnetic Fe₃O₄ nanoparticles on fluorescence quenching of dye molecules, *J. Nanosci. Nanotechnol.* **16** (2016) 7427-7432.

12. Hao C., Xu G., Feng Y., Lu L., Sun W. and Sun R. - Fluorescence quenching study on the interaction of ferroferric oxide nanoparticles with bovine serum albumin, *Spectrochim. Acta - Part A Mol. Biomol. Spectrosc* **184** (2017) 191-197.
<https://doi.org/10.1016/j.saa.2017.05.004>.
13. Brand L. and Johnson M. L., *An Introduction to Fluorescence Spectroscopy*, in: 2011, p. 15. <http://books.google.com/books?id=GgFXweh0hmQC&pgis=1>.
14. Bordbar A. K., Rastegari A. A., Amiri R., Ranjbakhsh E., Abbasi M., Khosropour A. R. - Characterization of Modified Magnetite Nanoparticles for Albumin Immobilization, *Biotechnol. Res. Int.* **2014** (2014) 1-6. <https://doi.org/10.1155/2014/705068>.
15. Nazanin H., Samantha G., Hongbin H., and Gang B. - The effect of nanoparticle size on in vivo pharmacokinetics and cellular interaction Nanoparticle-based, *Nanomedicine* **11** (2016) 673-692.